

Effect of γ -Al₂O₃/Water Nanofluid on Natural Convection Heat Transfer of Corrugated Γ Shaped Cavity: Study the Different Aspect Ratio of Grooves

R. Mohebbi^{1†}, S. Haghghi Khalilabad¹ and Y. Ma^{2,3}

¹*School of Engineering, Damghan University, P.O. Box: 3671641167, Damghan, Iran*

²*Shanghai Automotive Wind Tunnel Center, Tongji University, No.4800, Cao'an Road, Shanghai, China, 201804*

³*Shanghai Key Lab of Vehicle Aerodynamics and Vehicle Thermal Management Systems, No.4800, Cao'an Road, Shanghai, China, 201804*

†*Corresponding Author Email: rasul_mohebbi@du.ac.ir*

(Received July 26, 2018; accepted November 13, 2018)

ABSTRACT

In this paper, the effect of γ -Al₂O₃/water nanofluid on the flow pattern and natural convection heat transfer of corrugated Γ shaped cavity is investigated numerically by the Lattice Boltzmann Method (LBM). The effects of nanoparticles solid volume fraction ($\phi=0-0.006$), Rayleigh number ($Ra=10^3-10^6$) and the aspect ratio of grooves cavity ($h/H=0.05-0.15$) on the streamlines, isotherms and averaged Nusselt number have been examined. In addition, a comparison between γ -Al₂O₃/water nanofluid and MWCNT-Fe₃O₄/Water Hybrid Nanofluid on the average Nusselt number are studied. The results showed that the heat transfer rate of γ -Al₂O₃/water nanofluid is higher than water. For all Rayleigh numbers and solid volume fraction of nanoparticles, increasing the height of grooves leads to an increment in average Nusselt number. Moreover, when the Rayleigh number reaches to 10^6 , the average Nusselt number increases, which the domain mechanism of heat transfer, in this case, becomes convection. As to be expected, the influence of MWCNT-Fe₃O₄/Water Hybrid Nanofluid on heat transfer rate is higher than the γ -Al₂O₃/water nanofluid.

Keywords: Al₂O₃/water nanofluid; Γ Shaped cavity; Grooves; LBM.

NOMENCLATURE

AR	cavity aspect ratio	Ra	Rayleigh number
c_s	speed of sound	T	dimensional temperature
c_p	specific heat at constant pressure	t	time
d	length of corrugates	w	wall
e	streaming speed for single-particle		
F	external force	Subscripts	
f	density distribution function	c	cold
f^{eq}	equilibrium density distribution function	f	base fluid
g	energy distribution function	h	hot
g^{eq}	equilibrium energy distribution function	i	move direction of single-particle
H	height of the cavity	U,V	dimensionless velocity components
h	height of corrugates	u,v	velocity components
k	thermal conductivity	u	velocity vector
L	length of the cavity	X,Y	dimensionless Cartesian coordinates
s	width of the fin	x,y	Cartesian coordinates
M	number of lattices	W	width of the cavity
Ma	Mach number	w	weight function
Nu	Nusselt number		
nf	nanofluid	α	thermal diffusivity
p	nanoparticle	β	thermal expansion coefficient
P	dimensional pressure	μ	dynamic viscosity
Pr	Prandtl number	ϕ	volume fraction of particle

Table 1 Thermo-physical properties of γ -Al₂O₃/water nanofluid for different volume fraction. (Bayomy *et al.*, 2017)

Volume fraction	T (°C)	ρ_{nf} (Kg.m ⁻³)	k_{nf} (W.m ⁻¹ .K ⁻¹)	μ_{nf} (mp.s)	$C_{p\ nf}$ (J.Kg ⁻¹ .K ⁻¹)	Pr
$\phi=0.0$ (host fluid)	20	998.2	0.613	0.001002	4182	6.8358303
$\phi=0.001$	20	1000.802	0.614817	0.001007	4169.70865	6.8306128
$\phi=0.003$	20	1006.005	0.618523	0.001019	4145.31669	6.8281311
$\phi=0.006$	20	1013.811	0.624262	0.00104	4109.19825	6.84356

- There are no thermal dissipations due to viscous or magnetic forces within the nanofluid. (8)

- The density changes are estimated by Boussinesq model.

$$U \frac{\partial \theta}{\partial X} + V \frac{\partial \theta}{\partial Y} = \frac{\alpha_{nf}}{\alpha_f} \left[\frac{\partial^2 \theta}{\partial X^2} + \frac{\partial^2 \theta}{\partial Y^2} \right] \quad (9)$$

The dimensional governing equations are as the follows:

$$\frac{\partial u}{\partial x} + \frac{\partial v}{\partial y} = 0 \quad (1)$$

$$\rho_{nf} \left(u \frac{\partial u}{\partial x} + v \frac{\partial u}{\partial y} \right) = -\frac{\partial p}{\partial x} + \mu_{nf} \left(\frac{\partial^2 u}{\partial x^2} + \frac{\partial^2 u}{\partial y^2} \right) \quad (2)$$

$$\rho_{nf} \left(u \frac{\partial v}{\partial x} + v \frac{\partial v}{\partial y} \right) = -\frac{\partial p}{\partial y} + \mu_{nf} \left(\frac{\partial^2 v}{\partial x^2} + \frac{\partial^2 v}{\partial y^2} \right) + (\rho\beta)_{nf} g (T - T_c) \quad (3)$$

$$u \frac{\partial T}{\partial x} + v \frac{\partial T}{\partial y} = \alpha_{nf} \left[\frac{\partial^2 T}{\partial x^2} + \frac{\partial^2 T}{\partial y^2} \right] \quad (4)$$

Also, the non-dimensional parameters can be found as followings:

$$\begin{aligned} X &= \frac{x}{L}, Y = \frac{y}{L}, U = \frac{uL}{\alpha_f}, V = \frac{vL}{\alpha_f}, \\ AR &= \frac{W}{H}, P = \frac{\rho L^2}{\rho_{nf} \alpha_f^2}, \theta = \frac{T - T_c}{T_h - T_c}, \\ Ra &= \frac{g \beta_f H^3 (T_h - T_c)}{\alpha_f \nu_f}, Pr = \frac{\nu_f}{\alpha_f} \end{aligned} \quad (5)$$

Combination of the above parameters and Eqs. (1)–(4) the following dimensionless equations found:

$$\frac{\partial U}{\partial X} + \frac{\partial V}{\partial Y} = 0 \quad (6)$$

$$U \frac{\partial U}{\partial X} + V \frac{\partial U}{\partial Y} = -\frac{\partial P}{\partial X} + \frac{\mu_{nf} / \mu_f}{\rho_{nf} / \rho_f} Pr \left[\frac{\partial^2 U}{\partial X^2} + \frac{\partial^2 U}{\partial Y^2} \right] \quad (7)$$

$$U \frac{\partial V}{\partial X} + V \frac{\partial V}{\partial Y} = -\frac{\partial P}{\partial Y} + \frac{\mu_{nf} / \mu_f}{\rho_{nf} / \rho_f} Pr \left[\frac{\partial^2 V}{\partial X^2} + \frac{\partial^2 V}{\partial Y^2} \right] +$$

$$\frac{(\rho\beta)_{nf}}{\rho_{nf} \beta_f} Ra Pr \theta$$

Also, the non-dimensional boundary conditions are as follow:

$$\begin{cases} \text{on all walls: } U = V = 0 \\ \text{on hot walls: } \theta = 1 \\ \text{on cold walls: } \theta = 0 \\ \text{on adiabatic walls: } \partial\theta / \partial n = 0 \end{cases} \quad (10)$$

2.1 Thermophysical Properties of the Nanofluid

Tables 1 to 3 show the characteristics of different phases. For description the thermophysical properties of nanofluids, the following equations are used (Mohebbi, Lakzayi *et al.* (2018), Mohebbi, Rashidi *et al.* (2018):

The density of the nanofluid is:

$$\rho_{nf} = (1 - \Phi) \rho_f + \Phi \rho_s \quad (11)$$

where ϕ is the solid volume fraction of the nanoparticles and f , nf and p are represented the base fluid, nanofluid and nanoparticles, respectively. The heat capacity and volume expansion coefficient of the nanofluid are:

$$(\rho c_p)_{nf} = (1 - \phi)(\rho c_p)_f + \phi(\rho c_p)_p \quad (12)$$

$$(\rho\beta)_{nf} = (1 - \phi)(\rho\beta)_f + \phi(\rho\beta)_p \quad (13)$$

The thermal diffusivity α_{nf} and Prandtl number of nanofluid are as:

$$\alpha_{nf} = \frac{k_{nf}}{(\rho c_p)_{nf}} \quad (14)$$

$$Pr_{nf} = \frac{(\mu c_p)_{nf}}{k_{nf}} \quad (15)$$

The dynamic viscosity of the γ -Al₂O₃-water nanofluid defines by (Bayomy and Saghir, 2017):

$$\frac{\mu_{nf}}{\mu_f} = 1 + 4.93\phi + 222.4\phi^2 \quad (16)$$

Table 2 Thermo-physical properties of carbon nanotube-Fe₃O₄ hybrid nanofluid for different volume fraction and temperatures. (Sundar *et al.*, 2014)

Volume fraction	T (°C)	ρ_{nf} (Kg.m ⁻³)	k_{nf} (W.m ⁻¹ .K ⁻¹)	μ_{nf} (mp.s)	$C_{p,nf}$ (J.Kg ⁻¹ .K ⁻¹)	Pr
$\phi=0.0$ (host fluid)	20	998.5	0.602	0.79	4182	5.5
$\phi=0.001$	20	1002.34	0.6734	0.91	4182.66	5.64
$\phi=0.003$	20	1010.04	0.6856	1.01	4183.99.	6.10

Table 3 Thermophysical properties of γ -Al₂O₃, Fe₃O₄ and MWCNT

property	d_p (nm)	ρ (kgm ⁻³)	c_p (Jkg ⁻¹ k ⁻¹)	k (wm ⁻¹ k ⁻¹)	β (k ⁻¹)
γ - Al ₂ O ₃	50	3600	765	40	8.46×10^{-6}
Fe ₃ O ₄	30	5810	670	6	1.3×10^{-5}
MWCNT	30	2100	711	3000	4.2×10^{-5}

For the nanofluid's heat conductivity coefficient the following used:

$$\frac{k_{nf}}{k_f} = 1 + 2.944\phi + 19.672\phi^2 \quad (17)$$

For dynamic viscosity and nanofluid's heat conductivity coefficient of MWCNT-Fe₃O₄/water hybrid nanofluid please refer to (Sundar *et al.*, 2014).

2.2 LBM

The LBM with D2Q9 standard has been employed for solving the present problem (Nazari *et al.* 2014).

The lattice Boltzmann equation (LBE) with the external forces can be written as:

$$f_i(x + e_i\delta t, t + \delta t) - f_i(x, t) = -\frac{1}{\tau_v} [f_i(x, t) - f_i^{eq}(x, t)] + \Delta t \cdot F_i \cdot e_i \quad (i = 0, 1, \dots, 8) \quad (18)$$

where f is the density distribution function and Δt is the lattice time. The force term F_i defined by:

$$F_i = 3w_i \rho g_y \beta (T - T_m) \quad (19)$$

where ρ , g_y , β and T are the local density, gravitational acceleration, thermal expansion coefficient and the local temperature, respectively and the average temperature is $T_m = (T_h + T_c)/2$.

The relaxation time for the flow field, τ_v can be defined as (Ma *et al.* 2018):

$$\tau_v = 0.5 + \nu \frac{\delta t}{c_s^2} \quad (20)$$

where ν is the kinematic viscosity and the equilibrium distribution function, f_i^{eq} , defined by:

$$f_i^{eq} = w_i \rho \left[1 + 3 \frac{e_i \cdot u}{c^2} + \frac{9}{2} \frac{(e_i \cdot u)^2}{c^4} - \frac{3}{2} \frac{u^2}{c^2} \right] \quad (i = 0, 1, \dots, 8) \quad (21)$$

The value of weight function w_i are $w_0=4/9$, $w_i=1/9$ for $i=1$ to 4 and $w_i=1/36$ for $i=5$ to 8. The macroscopic values such as ρ , ρu , found by:

$$\rho = \sum_{i=0}^8 f_i \quad (22)$$

$$\rho u = \sum_{i=0}^8 f_i e_i \quad (23)$$

For the thermal field by definition the g as the energy distribution function, the LBE is:

$$g_i(x + e_i\delta t, t + \delta t) - g_i(x, t) = -\frac{1}{\tau_g} [g_i(x, t) - g_i^{eq}(x, t)] \quad (24)$$

where the relaxation time τ_g found by:

$$\tau_g = \frac{3k}{(\rho c_p)_f c^2 \delta t} + 0.5 \quad (25)$$

and the equilibrium energy distribution function, g_i^{eq} can be given as the following:

$$g_i^{eq} = w_i T \left[1 + 3 \frac{e_i \cdot u}{c^2} \right] \quad (26)$$

where the value of T is:

$$T = \sum_{i=0}^8 g_i \quad (i = 0, 1, \dots, 8) \quad (27)$$

Also, the viscosity is calculated by fixing the Mach number $Ma=0.1$, the number of lattices in the y -direction M , Rayleigh number and Prandtl number as:

Table 4 Grid study: $\phi=0.006, h/H=0.1, Ra=10^4$

Grid number	61×61	81×81	101×101	121×121
Nu _{avg}	3.7128	3.6576	3.5105	3.5049
Percentage of error (Nu _{new} -Nu _{old})×100/Nu _{new}		1.5091	4.1902	0.1597

$$v = \sqrt{\frac{Ma^2 M^2 Pr_c^2}{Ra}} \quad (28)$$

The local Nusselt number on the hot walls is:

$$Nu = -\frac{k_{mf}}{k_f} \frac{\partial \theta}{\partial n} \quad (29)$$

So that, the averaged Nusselt number is obtained by integrating along the hot walls. For all the walls, the Bounce-back scheme has been used (Zou *et al.*, 1997; Inamuro, 1995). (Mohammad, 2011)'s method used for hot, cold and adiabatic boundary conditions.

3. GRID INDEPENDENCY AND CODE VALIDATION

Table 4 shows the grid-independence test for four different grid study. The average Nusselt number for these meshes indicated that there is a little relative error (0.1597 percentage) between the grid sizes 101×101 and 121×121. Hence, the 101×101 grid size is appropriate for this study.

In order to test the validity of the present code, a comparison done against the work of Nithiarasu *et al.* (1998) within a Γ shaped cavity as shown in Figs. 2 and 3. The results indicate that the present code is accurate for this study.

4. RESULTS AND DISCUSSION

Fluid flow and heat transfer inside a corrugated Γ shaped cavity filled with γ -Al₂O₃/water nanofluid are studied using LBM. The effect of aspect ratio of grooves on flow pattern and heat transfer characteristics is examined for Rayleigh number between 10³ and 10⁶, the height of grooves between 0.05H to 0.15H, nanoparticle volume fraction between 0 and 0.06 and for two kinds of the nanoparticle.

Figures 4 and 5 show the effect of adding nanofluid in the base fluid on streamlines and isotherms at h/H=0.1 for different Rayleigh numbers, respectively. As shown in Fig. 4, at Ra=10³, a large vortex occupies the right vertical part of the cavity, and the fluid in the vertical part is almost stationary. As the Rayleigh number increases to 10⁴, the flow pattern changes slightly and the streamlines follow the shape of the enclosure. For Ra=10⁵, the flow intensity rises

significantly and four vortices are established in the horizontal part of the enclosure. Moreover, three secondary vortices are created inside the largest vortex located in the right part of the enclosure. When the Rayleigh number increases to 10⁶ from 10⁵, the vortices inside the enclosure become stronger. The increase in Rayleigh number leads to the rise of the buoyancy force, as a result, the fluid movement is developed.

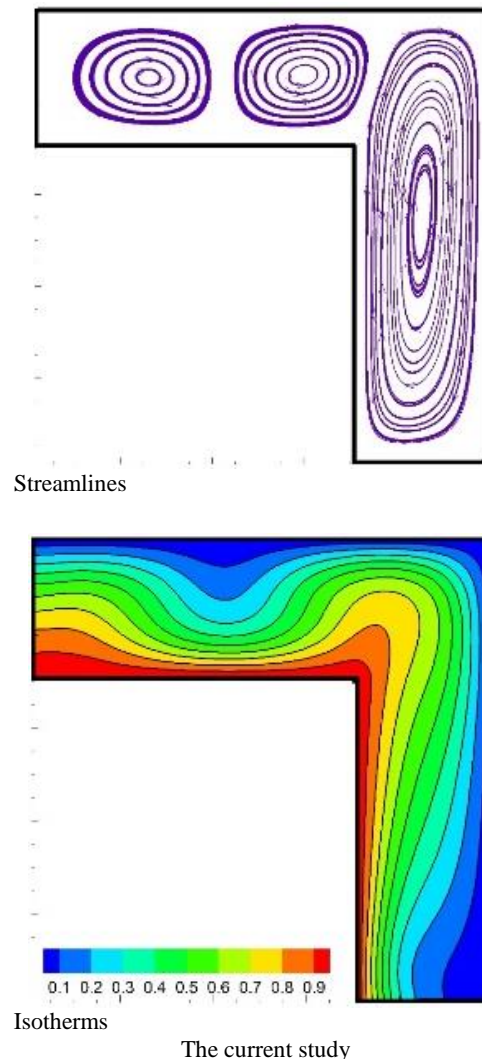
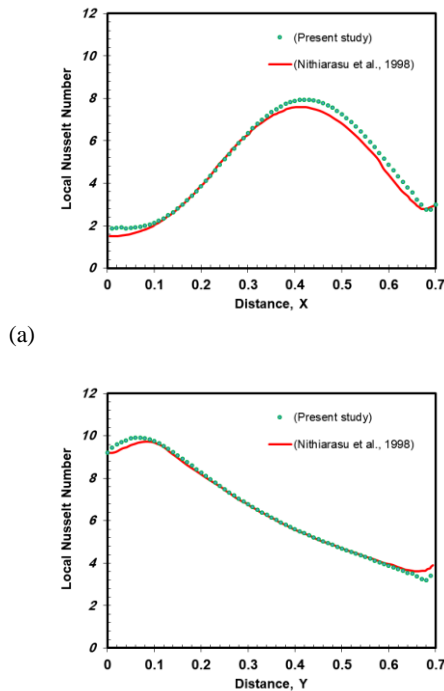


Fig. 2. Streamlines and isotherms of the current study under the conditions in Nithiarasu *et al.* (1998) study.



(a)
(b)
Fig. 3. Comparison of the local Nusselt number along the (a): hot horizontal wall (b): hot vertical wall for the present study and Nithiarasu *et al.* (1998) at $Ra=10^5$.

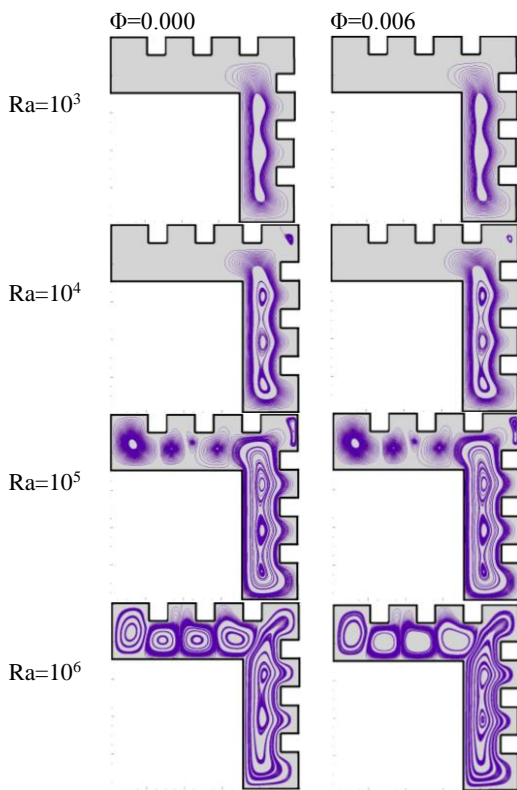


Fig. 4. Streamlines of $\Phi=0.000$ and 0.006 at different Rayleigh numbers for $h/H=0.1$.

As it can be seen in Fig. 5, by adding the nanoparticles, the change of the heat transfer

characteristics does not change significantly. When the Rayleigh number is 10^3 , the isotherm lines are flat and parallel to each other and does not follow the shape of the grooves. In this Rayleigh number, the conduction mechanism is more significant than the convection one. As the Rayleigh number increases to 10^4 or 10^5 , the isotherms change slightly and the isotherms adjacent to the hot wall is also even, however, the isotherms near the cold corrugated wall become rugged. As for $Ra=10^6$, the thermal plumes can be found above the horizontal hot wall and limping to the corrugated cold walls. As a result, the thermal boundary layer of the cold walls decreases. Also, for this Rayleigh number, the domain heat transfer mechanism is natural convection.

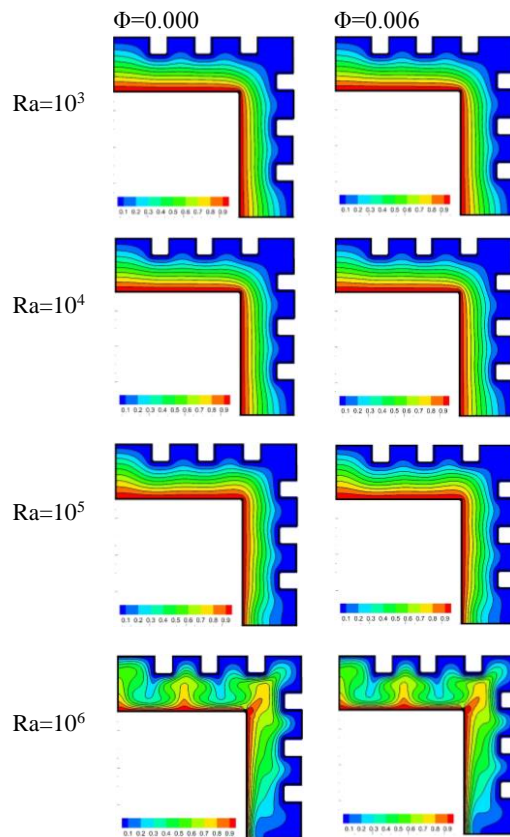


Fig. 5. Isotherms of $\Phi=0.000$ and 0.006 at different Rayleigh numbers for $h/H=0.1$.

Figure 6 shows the streamlines of nanofluid within the enclosure for different height of grooves at different Rayleigh numbers. It was evident that the effect of the groove's height on flow pattern at low Rayleigh number (10^3) is very weak. This is due to that at low Rayleigh numbers, the convection heat transfer mechanism is not primary. Thus, the effect of groove height on natural convection is also not noticeable. However, at $Ra=10^6$, the increase of the groove height affects the flow pattern distinctly. When the height of the grooves increases, the fluid movement is restrained and the vortices are squeezed. Especially for $h/H=0.15$, the largest vortex located in the right vertical part of the enclosure follows the shape of the corrugated cold wall.

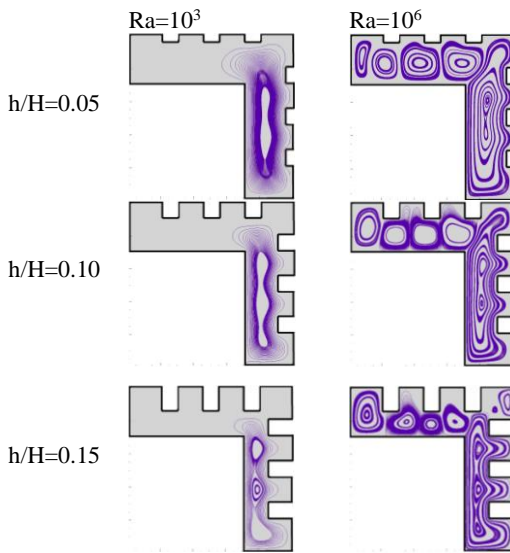


Fig. 6. Streamlines of nanofluid ($\phi = 0.006$) inside the enclosure for different height of grooves and various Rayleigh number.

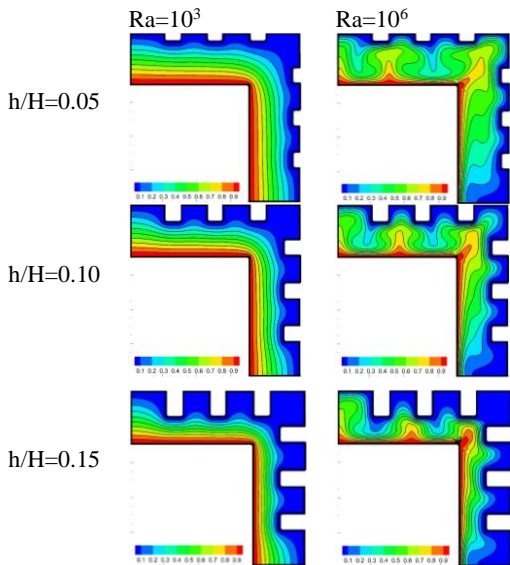


Fig. 7. Isotherms of nanofluid ($\phi = 0.006$) inside the enclosure for different height of grooves and various Rayleigh number.

Figure 7 illustrates the effect of groove's height on isotherms at different Rayleigh numbers for $\phi=0.006$. At $Ra=10^3$, due to the conduction-domain heat transfer mechanism, the isotherms change slightly when the height of grooves increases from $0.05H$ to $0.15H$ and the isotherms are parallel to each other. As for $Ra=10^6$, when the height of the grooves is $0.05H$, the thermal plume in the left horizontal part of the enclosure is large and the isotherms in the right vertical part are crooked and irregular. As the groove's height increases to $0.1H$, the thermal plume becomes smaller because of the suppression of the small gap between the cold and hot walls. Moreover, the isotherms in the right regime of the enclosure become even. At $h/H=0.15$, the thermal plume above the horizontal

hot wall is tiny. The isotherms adjacent to the vertical hot wall are almost straight lines and they become more crowded significantly.

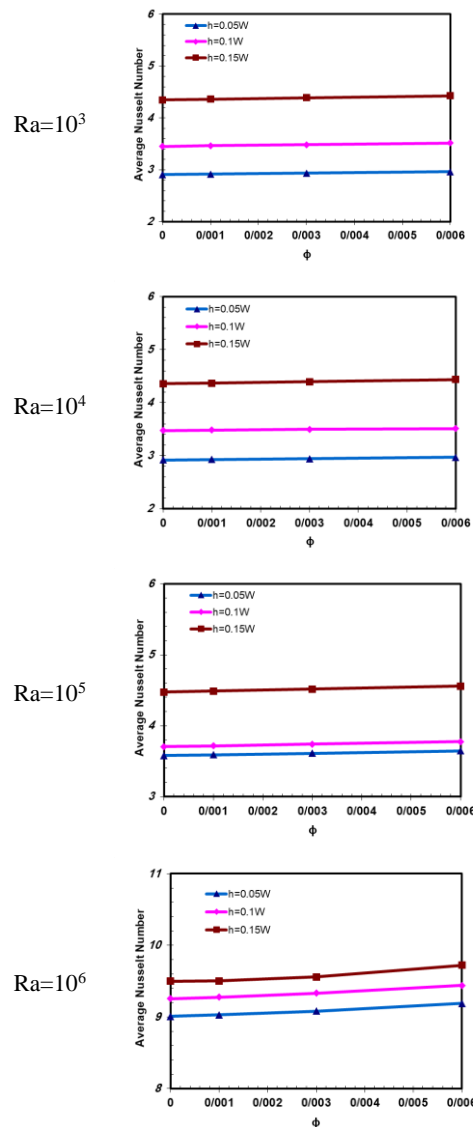


Fig. 8. Variation of average Nusselt number at different solid volume fraction an Rayleigh number at various height of grooves.

Figure 8 shows the variation of the average Nusselt number of the hot walls versus the nanoparticle volume fraction for different height of grooves at different Rayleigh numbers. It was evident that in all cases, the average Nusselt number increases linearly as increasing the volume concentration and has the maximum value at $\phi = 0.06$. It can be concluded that the heat transfer rate of $\gamma\text{-Al}_2\text{O}_3$ /water nanofluid is higher than that of pure water, which is due to the high thermal conductivity of nanoparticles. Moreover, for every Rayleigh number and volume fraction of nanoparticle, when increasing the height of the grooves, the average Nusselt number increases and the maximum can be obtained at $h=0.15W$. This is because that as increasing the groove height, the

temperature gradient on hot surfaces is increased, which lead to that the convection heat transfer is more primary than conduction and the rate of heat transfer increases.

The averaged Nusselt number distribution on the hot walls with the Rayleigh number for different groove height at different nanoparticle volume fractions are shown in Fig. 9. It can be seen, in all cases, when the Rayleigh number increases from 10^3 to 10^5 , the average Nusselt number changes slightly, which is due to that the heat transfer mechanism with the range of $10^3 \leq Ra \leq 10^5$ is conduction-domain mechanism and when the Rayleigh number increases to 10^6 , the domain heat transfer mechanism becomes convection heat transfer. Also, the rate of heat transfer is bigger at $\phi=0.006$.

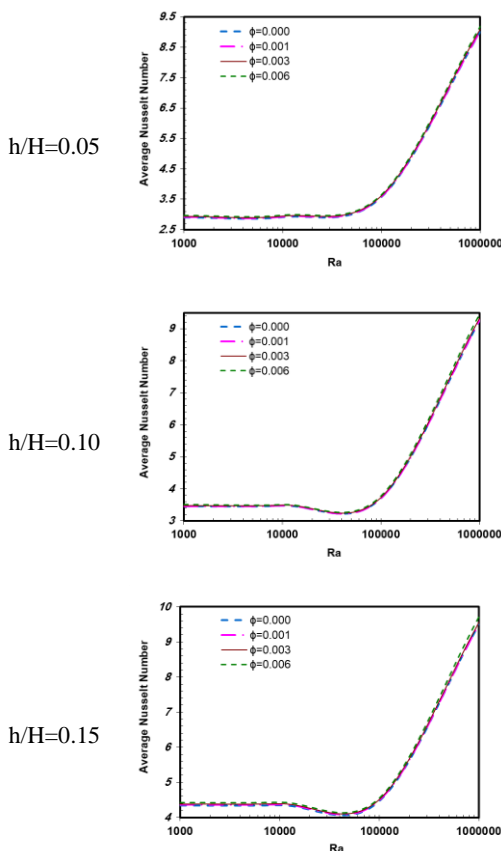


Fig. 9. Variation of the average Nusselt number at different Rayleigh numbers and solid volume fraction at various height of grooves.

The effects of two kinds of nanoparticles and the nanoparticle volume fraction on the averaged Nusselt number at different Rayleigh numbers are illustrated in Fig. 10. It is distinct that comparing with the pure fluid, the effect of MWCNT-Fe₃O₄/water nanofluid on heat transfer is same to γ -Al₂O₃/water nanofluid. However, at each nanoparticle volume fraction, the heat transfer enhancement of MWCNT-Fe₃O₄/water is more effective than that of γ -Al₂O₃/water nanofluid.

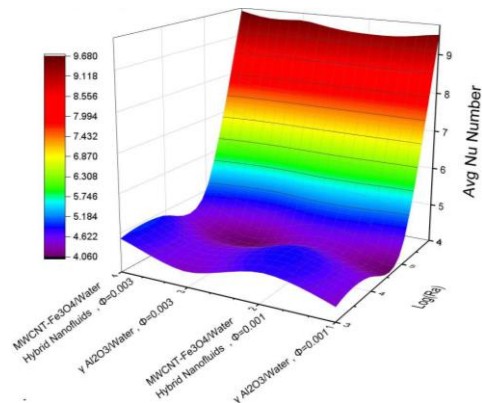


Fig. 10. Variation of average Nusselt number for different kinds of nanofluid at different Rayleigh numbers.

5. CONCLUSION

In this paper, the natural convection heat transfer of corrugated Γ shaped cavity filled with nanofluid studied using LBM. The effects of γ Al₂O₃/water nanofluid and aspect ratio of grooves on flow pattern and heat transfer characteristics are investigated. Different parameters like Rayleigh number, the height of grooves and nanoparticle volume fraction have been examined. Using an overview of the figures and tables following items can be concluded:

- Adding nanoparticles to the working fluid leads to a higher heat transfer rate, which is due to the high thermal conductivity of nanoparticles.
- For every Rayleigh number and volume fraction of nanoparticle, the increment of the height of grooves increases the average Nusselt number because of an enhancement of the hot surface and the temperature gradient.
- At the range of low value of Rayleigh numbers, averaged Nusselt number changes slightly while its range increased considerably at a higher value of Rayleigh numbers.

REFERENCES

Abouei Mehrizi, A., M. Farhadi, K. H. Hassanzade Afroozi, K. Sedighi, A.A. Rabiataj Darz (2012). Mixed convection heat transfer in a ventilated cavity with a hot obstacle: effect of nanofluid and outlet port location. *International Communication of Heat and Mass Transfer* 39 (7), 1000–1008.

Abu-Nada, E. and A.J. Chamkha (2010). Mixed Convection Flow in a Lid-Driven Inclined Square Enclosure Filled with a Nanofluid. *European Journal of Mechanics B/Fluids* 29, 472-482.

Bayomy, A. M. and M. Z. Saghir (2017). Experimental study of using γ -Al₂O₃-water nanofluid flow through aluminum foam heat sink: comparison with numerical approach. *International Journal of Heat and Mass*

- Transfer* 107, 181-203.
- Chen, S. and G. D. Doolen (1998). Lattice Boltzmann method for fluid flows. *Annual review of fluid mechanics* 30(1), 329-364.
- Choi, S. U. S. and J. A. Eastman (1995). Enhancing Thermal Conductivity of Fluids with Nanoparticles. In *Proceeding of the 1995 ASME International Mechanical Engineering Congress and Exposition*, San Francisco, USA, ASME, FED 231/MD 66, 99-105.
- Fattahi, E., M. Farhadi, K. Sedighi and H. Nemati (2012). Lattice Boltzmann Simulation of Natural Convection Heat Transfer in Nanofluids. *International Journal of Thermal Sciences* 52, 137-144.
- Freidoonimehr, N., M.M. Rashidi and S. Mahmud (2015). Unsteady MHD free convective flow past a permeable stretching vertical surface in a nano-fluid. *International Journal of Thermal Sciences* 87, 136-145.
- Hu, Y., D. Li, S. Shu and X. Niu (2017). Lattice Boltzmann simulation for three-dimensional natural convection with solid-liquid phase change. *International Journal of Heat and Mass Transfer* 113, 1168-1178.
- Inamuro, T., M. Yoshino and F. Ogino (1995). A non-slip boundary condition for lattice Boltzmann simulations. *Physics of Fluids* 7(12), 2928-2930.
- Izadi, M., G. Hoghoughi, R. Mohebbi and M. Sheremet (2018). Nanoparticle migration and natural convection heat transfer of Cu-water nanofluid inside a porous undulant-wall enclosure using LTNE and two-phase model. *Journal of Molecular Liquids* 261, 357-372.
- Izadi, M., R. Mohebbi, D. Karimi and M. A. Sheremet (2018). Numerical Simulation of Natural Convection Heat Transfer inside a Contrariwise T-Shaped Cavity Filled by an MWCNT-Fe₃O₄/Water Hybrid Nanofluids using LBM. *Chemical Engineering & Processing: Process Intensification* 125, 56-66.
- Kalidasan, K. and P. R. Kanna (2016). Effective utilization of MWCNT-water nanofluid for the enhancement of laminar natural convection inside the open square enclosure. *Journal of the Taiwan Institute of Chemical Engineers* 65, 331-340.
- Kefayati, GH. R., S.F. Hosseinzaeh, M. Gorji and H. Sajjadi (2011). Lattice Boltzmann simulation of natural convection in tall enclosures using water/SiO₂ nanofluid. *International Communications in Heat and Mass Transfer* 38, 798-805.
- Khanafar, K., K. Vafai and M. Lightstone (2003). Buoyancy-driven heat transfer enhancement in a two-dimensional enclosure utilizing nanofluids. *International Journal of Heat and Mass Transfer* 46 (19), 3639-3653.
- Krüger, T., H. Kusumaatmaja, A. Kuzmin, O. Shardt, G. Silva and E. M. Viggien (2017). *The Lattice Boltzmann Method*. Springer.
- Ma, Y., R. Mohebbi, M. M. Rashidi and Z. Yang (2018). Numerical Simulation of Flow Over a Square Cylinder with Upstream and Downstream Circular Bar Using Lattice Boltzmann Method. *International Journal of Modern Physics C* 29(4).
- Ma, Y., R. Mohebbi, M. M. Rashidi and Z. Yang (2018). Study of Nanofluid Forced Convection Heat Transfer in a Bent Channel by Means of Lattice Boltzmann Method. *Physics of Fluids* 30 (3).
- Ma, Y., R. Mohebbi, M. M. Rashidi and Z. Yang (2019). Effect of Hot Obstacle Position on Natural Convection Heat Transfer of MWCNTs-Water Nanofluid in U-Shaped Enclosure Using Lattice Boltzmann Method, *International Journal of Numerical Methods for Heat and Fluid Flow* 29(1), 223-250.
- Maxwell, J.C. (1873). *A Treatise on Electricity and Magnetism*, Clarendon Press, Oxford.
- Mohamad, A. A. (2011). *Lattice Boltzmann Method Fundamentals and Engineering Applications with Computer Codes*. Springer
- Mohebbi, R and H. Heidari (2017). Lattice Boltzmann simulation of fluid flow and heat transfer in a parallel-plate channel with transverse rectangular cavities. *International Journal of Modern Physics C* 28(03), 1750042.
- Mohebbi, R, M. Nazari and M. H. Kayhani (2016). Comparative Study of Forced Convection of a Power-Law Fluid in a Channel with a Built in Square Cylinder. *Journal of Applied Mechanics and Technical Physics* 57(1), 55-68.
- Mohebbi, R. and M. M. Rashidi (2017). Numerical simulation of natural convection heat transfer of a nanofluid in an L-shaped enclosure with a heating obstacle. *Journal of the Taiwan Institute of Chemical Engineers* 72, 70-84.
- Mohebbi, R., H. Lakzayi, N. A. C. Sidik and W. M. Arif Aziz Japaret (2018). Lattice Boltzmann method based study of the heat transfer augmentation associated with Cu/water nanofluid in a channel with surface mounted blocks. *International Journal of Heat and Mass Transfer* 117, 425-435.
- Mohebbi, R., M. M. Rashidi, M. Izadi, N. A. C. Sidik and H. W. Xian (2018). Forced Convection of Nanofluids in an Extended Surfaces Channel using Lattice Boltzmann Method. *International Journal of Heat and Mass Transfer* 117, 1291-1303.
- Nazari, M, M. H. Kayhani and R. Mohebbi (2013). Heat transfer enhancement in a channel partially filled with a porous block: lattice Boltzmann method. *International Journal of Modern Physics C* 24(09), 1350060.

- Nazari, M., R. Mohebbi and M. H. Kayhani (2014). Power-law fluid flow and heat transfer in a channel with a built-in porous square cylinder: Lattice Boltzmann simulation. *Journal of non-Newtonian fluid mechanics* 204, 38-49.
- Nithiarasu, P., T. Sundararajan and K. N. Seetharamu (1998). Finite element analysis of transient natural convection in an odd-shaped enclosure. *International Journal of Numerical Method for Heat and Fluid Flow* 8 (2), 199–216.
- Qi, C., G. Wang, L. Yang, Y. Wan and Z. Rao (2017). Two-phase lattice Boltzmann simulation of the effects of base fluid and nanoparticle size on natural convection heat transfer of nanofluid. *International Journal of Heat and Mass Transfer* 105, 664-672.
- Syam Sundar, L., M. K. Singh and A. C. M. Sousa (2014). Enhanced heat transfer and friction factor of MWCNT–Fe₃O₄/water hybrid nanofluids. *International Communications in Heat and Mass Transfer* 52, 73–83.
- Zou, Q. and X. He (1997). On pressure and velocity boundary conditions for the lattice Boltzmann BGK model. *Physics of Fluids* 9(6), 1591-1598.